Investigation of total reaction cross sections for proton-dripline nuclei ^{17}F and ^{17}Ne on a proton target

T. Moriguchi [1,*] R. Kagesawa,[1] A. Ozawa,[1] W. Horiuchi [2,3,4,5] Y. Abe,[4] M. Amano,[1]
D. Kamioka,[1] A. Kitagawa,[6] M. Mukai [7] D. Nagae,[4,8] M. Sakaue,[9] S. Sato,[6] B. H. Sun,[10]
S. Suzuki,[11] T. Suzuki [9] T. Yamaguchi [9] A. Yano [1] and K. Yokota[9]

[1]*Institute of Physics, University of Tsukuba, Ibaraki 305-8571, Japan*
[2]*Department of Physics, Osaka Metropolitan University, Osaka 558-8585, Japan*
[3]*Nambu Yoichiro Institute of Theoretical and Experimental Physics (NITEP), Osaka Metropolitan University, Osaka 558-8585, Japan*
[4]*RIKEN Nishina Center, Wako, Saitama 351-0198, Japan*
[5]*Department of Physics, Hokkaido University, Sapporo 060-0810, Japan*
[6]*National Institutes for Quantum Science and Technology, Chiba 263-8555, Japan*
[7]*Wako Nuclear Science Center (WNSC), Institute of Particle and Nuclear Studies (IPNS), High Energy Accelerator Research Organization (KEK), Ibaraki 305-0801, Japan*
[8]*Laboratory for Zero-Carbon Energy, Tokyo Institute of Technology, 2-12-1 Ookayama, Meguro-ku, Tokyo 152-8550, Japan*
[9]*Department of Physics, Saitama University, Saitama 338-8570, Japan*
[10]*School of Physics, Beihang University, Beijing 100191, China*
[11]*Japan Synchrotron Radiation Research Institute, Hyogo 679-5198, Japan*

(Received 16 January 2024; accepted 3 June 2024; published 8 July 2024)

We measured the total reaction cross section (σ_R) for the proton-dripline nucleus ^{17}F using a solid hydrogen target. Comparing the experimental results of ^{17}F and ^{17}Ne, σ_R on a proton target shows that the contribution of the isospin asymmetry of the nucleon-nucleon total cross section is more prominent than the changes in the nuclear radii of the two nuclei, while for a carbon target, the cross section simply reflects the nuclear matter radii of these isotopes, which are consistent with the results of previous theoretical works. The experimental values of σ_R for ^{17}F on a proton target at energies of several tens MeV/nucleon (several hundreds MeV/nucleon) are smaller (larger) than the theoretical values of σ_R; similar trend is observed for ^{17}Ne. This discrepancy is not resolved at this time; therefore, further studies of the experimental and theoretical sides are required to precisely understand nucleus-proton collisions.

DOI: 10.1103/PhysRevC.110.014607

I. INTRODUCTION

It is important to determine the proton- and neutron-distribution radii of atomic nuclei to precisely understand the nuclear halo and skin structure, which are known as characteristic phenomena of exotic nuclei located around the proton and neutron driplines. Measurement of the total reaction cross section (σ_R) is an effective method for investigating nuclear size properties such as radii and density distributions [1–8]. In particular, the use of a proton target for σ_R measurements has the advantage of the separation of the proton (ρ_p) and neutron (ρ_n) density distributions of a projectile nucleus [9,10]. This separation is based on the isospin asymmetry of the nucleon–nucleon total cross section ($\sigma_{NN}^{\rm tot}$), i.e., $\sigma_{pn}^{\rm tot}$ is around three times larger than $\sigma_{pp}^{\rm tot}$ below $\approx$100 MeV/nucleon [11]. This property shows that a proton target is more sensitive to ρ_n of a projectile nucleus than to ρ_p at low incident energies. A proton target also has a possibility to extract the nuclear size of medium and heavy nuclei properly because the contribution of Coulomb breakup to σ_R is sufficiently small, which helps to reduce the uncertainties in the reaction model [12]. Recently, the extraction of σ_R on a neutron target has been theoretically proposed by measuring σ_R for proton and deuteron targets [13]. By combining σ_R on proton and neutron targets, it is expected that the neutron-skin thickness can be determined more precisely than by utilizing the combination of σ_R on carbon and proton targets.

The root-mean-square (rms) proton radius (r_p) and ρ_p of a projectile nucleus can also be derived from measurements of the total charge-changing cross section (σ_{cc}) based on the sensitivity of the charge-changing reactions to ρ_p [14–23]. This method has been mainly applied to stable and neutron-rich nuclei. However, the experimental analysis becomes more complicated than that required for σ_R, e.g., an energy dependent factor is introduced into σ_{cc} to account for the difference between the theoretical and experimental cross sections [14,15]. Recently, the importance of the charged-particle evaporation effect was pointed out to explain the experimental σ_{cc} for stable and neutron-rich nuclei [24]. According to Ref. [24], the sensitivity of σ_{cc} to ρ_p is lower for nuclides near the beta-stability line compared with neutron-rich nuclei.

*Contact author: moriguchi@tac.tsukuba.ac.jp

Therefore, for proton-rich nuclei, it is difficult to extract ρ_p from σ_{cc} measurements because σ_{cc} comes close to σ_R toward the proton-dripline. In this case, σ_{cc} no longer reflects the proton distribution of the projectile nucleus.

As described above, measurements of σ_R on a proton target have many advantages in determining the nuclear size properties of unstable nuclei. In this study, we measured σ_R for ^{17}F on a proton target to investigate the collision between ^{17}F and a proton. We used a thick and large solid hydrogen target (SHT), developed for σ_R measurements with rare radioactive isotope beams [25]. ^{17}F ($T_{1/2} = 64.49(16)$ s [26]) is a proton-dripline nucleus of the fluorine isotopes. The one-proton separation energy of the ground state ($J^\pi = 5/2^+$) is small ($S_p = 600.27(25)$ keV [27]), and the existence of a proton skin was pointed out from several experimental and theoretical studies [28–32]. Measurements of interaction cross section (σ_I) at ≈700 MeV/nucleon revealed that the rms matter radius (r_m) of ^{17}F is not as large as that of proton-halo nuclei [33], whereas a proton-halo structure of the first excited state ($J^\pi = 1/2^+$) has been suggested [34,35]. The skin thickness of ^{17}F was not determined experimentally because the values of r_p and the rms neutron radius (r_n) of ^{17}F were unknown at that time.

The energy dependence of the total reaction cross sections on a proton target is not yet fully understood. Previously, we measured σ_R for ^{17}Ne using the SHT, and found that the theoretical cross sections overestimate the experimental ones in the low energy region (≈100 MeV/nucleon), whereas the theoretical ones significantly underestimate the experimental data in the intermediate energy region (≈400 MeV/nucleon) [36]. Further, theoretical studies show that σ_R on a proton target decreases for light proton-rich nuclei despite the increase of r_m toward the proton-dripline [37,38]. Here, by comparing experimental results and theoretical calculations for ^{17}F and ^{17}Ne, we discuss the energy dependence of σ_R on a proton target and the relation between nuclear size and σ_R.

This paper is organized as follows. In Sec. II, we describe the details of the experimental setup. In Sec. III, the data analysis for σ_R and experimental results are presented. In Sec. IV, we discuss the experimental σ_R on a proton target using the Glauber model. By comparing σ_R of the proton-dripline nuclei ^{17}F and ^{17}Ne, we discuss the target dependence of the relation between σ_R and nuclear size. We also discuss the energy dependence of σ_R for ^{17}F on a proton target. Finally, we summarize the paper in Sec. V.

II. EXPERIMENT

The experiment was performed using a fragment separator called SB2 [39] in the Heavy Ion Medical Accelerator in Chiba (HIMAC). The beam line settings are almost the same as those in our previous study (see Fig. 1 in Ref. [36]). A secondary beam was produced by bombarding a beryllium target (9–38 mm thick) located at the entrance of the separator (F0) with a ^{20}Ne beam. To measure the wide energy dependence of σ_R, we used beams with the energies 180, 290, 400, and 600 MeV/nucleon. ^{17}F particles were separated from other nuclei and identified using magnetic rigidity ($B\rho$), time of flight (TOF), and energy loss (ΔE). Aluminum-wedge energy degraders (7.055, 13.5, and 25.5 mm in central thickness) and a plastic scintillation counter (1.0 mm thick) for the TOF start signal were installed at the momentum dispersive focal plane (F1). A silicon detector (325 μm thick) was installed at the second focal plane (F2) to determine ΔE.

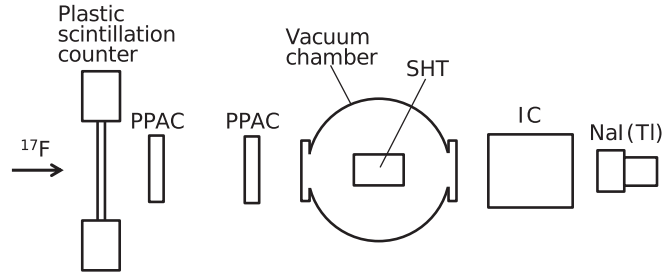

FIG. 1. Schematic view of the experimental setup around the reaction target.

Figure 1 shows the experimental setup around the reaction target downstream of the vacuum window (Al, 0.1 mm thick). The plastic scintillation counter shown in Fig. 1 was used as the TOF stop signal and as the trigger for data acquisition. Two parallel-plate avalanche counters (PPACs) [40] were used to determine the beam trajectory. As the reaction target, we used the SHT which is dedicated for σ_R measurements [25]. The SHT was located in a vacuum chamber with entrance and exit windows for the beams (Mylar, 100 μm thick). The SHT, which is surrounded by a copper cell, is cylindrically shaped with 50-mm-diameter entrance and exit windows of Kapton films (25 μm thick), and the thickness of the SHT can be changed by varying the length of the target cell. In this study, we used 30-mm-thick and 100-mm-thick SHTs, depending on the beam energy. The ionization chamber (IC) [41], which was filled with P10 gas (Ar 90% + CH_4 10% at ≈760 Torr), was used to measure ΔE for the identification of the atomic numbers of the outgoing particles from the SHT. Output signals from the IC were obtained from eight anode foils (4 μm thick, both sides aluminized Mylar). A NaI(Tl) scintillation counter (ϕ3 in., 60 mm thick) was used to measure the total energy (E).

We performed target-out measurements with an empty cell to enable us to subtract the particles produced by reactions with materials other than the SHT, such as air, foils, and detectors. In the target-out measurements, we adjusted the beam energies so as to match those of the target-in measurements because both measurements should have the same reaction rates. The experimental conditions for the production of ^{17}F are listed in Table I.

III. ANALYSIS AND RESULTS

Using the transmission method, σ_R can be obtained from the following equation:

$$\sigma_R = -\frac{1}{N_t} \ln\left(\frac{R_{in}}{R_{out}}\right), \quad (1)$$

where R_{in} is the ratio of the number of nonreacting particles (N_o) to that of incident particles (N_i) for a target-in

TABLE I. Experimental conditions for the production of ^{17}F. The energies of ^{17}F are given for the middle of the target. Typical values of the purity (%) and the intensity are listed, for which the unit is particles per pulse (ppp). The values in parentheses in the last column indicate the thickness of the SHT. Note that the difference in the purity between Nos. 2 and 4 is due to the magnetic field applied to the fragment separator.

^{17}F energy (MeV/nucleon)	Data number	^{20}Ne energy (MeV/nucleon)	Be (mm thick)	Degrader (mm thick)	Purity (%)	Intensity (ppp)	SHT (mm thick)
66	No. 1	180	9	7.055	70	200	In (30)
	No. 2	180	12	7.055	60	300	Out
97	No. 3	290	37	7.055	80	650	In (100)
	No. 4	180	12	7.055	70	300	Out
282	No. 5	400	20	13.5	50	550	In (100)
	No. 6	400	32	13.5	65	700	Out
461	No. 7	600	25	25.5	95	550	In (100)
	No. 8	600	38	25.5	95	700	Out

measurement and $R_{\rm out}$ is the same ratio but for the target-out measurement. Note that in the present analysis, we neglect inelastic scattering events, which cannot be identified in the present experiment, because the inelastic scattering cross section is negligible according to the theoretical calculations (see Sec. IV A). We analyzed the experimental data listed in Table I and obtained σ_R at 66, 97, 282, and 461 MeV/nucleon, where the beam energies of ^{17}F were defined at the middle of the SHT. Figure 2 shows a particle identification (PID) plot obtained using TOF and ΔE upstream of the SHT. This PID plot was constructed after selecting the beam position and angle to verify the full transmission of ^{17}F from the SHT to the IC using the two PPACs. The main product was ^{17}F, while small number of other nuclei were also found. ^{17}F events shown in Fig. 2 were projected onto the TOF and ΔE axes, and Gaussian fits were performed for each projection. To obtain $N_{\rm i}$, we counted the number of ^{17}F particles within a gate of $\pm 2\sigma$ ($G_{\rm up}$). Downstream of the SHT, we identified noninteracting ^{17}F using ΔE provided by the IC. Figure 3 shows typical ΔE spectra for the outgoing particles downstream of

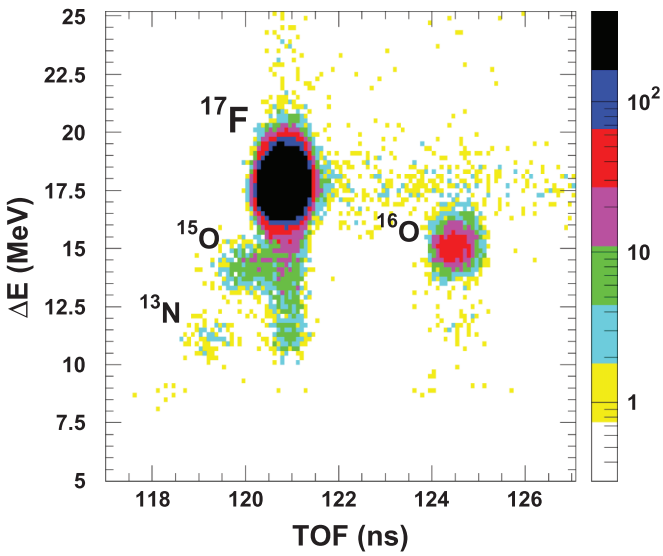

FIG. 2. Two-dimensional TOF–ΔE PID plot upstream of the SHT for ^{17}F at 282 MeV/nucleon. The intensity is color coded.

the SHT in the target-in and target-out measurements under the selection of ^{17}F particles upstream of the SHT within $G_{\rm up}$. The main peak in Fig. 3(a) corresponds to noninteracting ^{17}F, and other peaks correspond to reaction events that produced carbon, nitrogen, and oxygen isotopes. Since ^{17}F is the proton-dripline nucleus of the fluorine isotopes, its atomic number always changes, even when only the neutron-removal reaction occurs. Neutron-pickup reactions are negligible because we used pure hydrogen as the reaction target in this study. Therefore, noninteracting ^{17}F can be identified using the only ΔE. As shown in Fig. 3(b), almost all outgoing particles in the target-out measurement are noninteracting ^{17}F particles. We performed a Gaussian fit to the peak of the noninteracting ^{17}F and established a gate from -3σ to $+5\sigma$ ($G_{\rm down}$), which is indicated by the hatched area in Fig. 3. We counted the numbers of the ^{17}F peak within $G_{\rm down}$ to obtain $N_{\rm o}$. Note that in the target-in measurements at 66 and 97 MeV/nucleon, we subtracted the events corresponding to oxygen isotopes within $G_{\rm down}$ before counting $N_{\rm o}$. By performing a double Gaussian fit to the oxygen and ^{17}F peaks, we estimated the fraction of contaminants in $G_{\rm down}$ to be $\approx$0.7% of the number of reaction events. The analysis of the target-out measurements was the same as that of the target-in measurements but without the subtraction of oxygen contaminants, because this contribution was estimated to at most 0.1 mb.

The thickness of the SHT depends on the beam position because of the swelling of the thin Kapton films used for the entrance and exit windows. This swelling is caused by the pressure difference between the inside and outside of the cell during the growth of solid hydrogen. The curvature of the swelling is approximately expressed by a second-order polynomial function, which we determined empirically in the previous study [25]. In the present study, the effective thickness taken into account the statistical weight of the beam position at the SHT was used as the $N_{\rm t}$ in Eq. (1). In Ref. [25], we repeated solidification and melt, and measured the expansion of windows each time by the laser distance meter. From these measurements, we observed 2.55 mm for the sum of the expansion at the center of both the entrance and exit windows, and confirmed the reproducibility within the uncertainty of 0.26 mm. This uncertainty was used as the systematic one of the SHT thickness in the present study because all

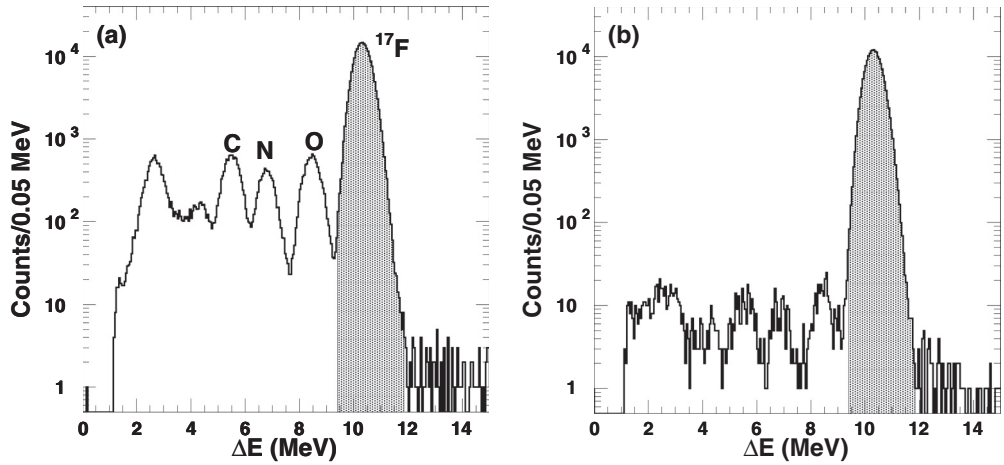

FIG. 3. Typical ΔE spectrum downstream of the SHT in (a) target-in and (b) target-out measurements for σ_R of ^{17}F at 289 MeV/nucleon. The numbers of noninteracting ^{17}F particles, which are indicated by the hatched area, were counted to determine the N_o.

conditions of the present SHT system are the same as those in Ref. [25].

The experimental results are listed in Table II along with the data numbers from Table I that we used in determining each σ_R for ^{17}F. In this study, we were able to measure the energy dependence of σ_R for ^{17}F on a proton target over a wide energy range. The statistical uncertainties were typically less than 0.7%, but around 1.1% at the energy 66 MeV/nucleon. The systematic uncertainties were mainly those of the SHT thickness and the molar volume of solid hydrogen [42]. The systematic ones of the SHT thickness were 0.9% and 0.3% for the 30 and 100 mm thick cases, respectively, which were derived from the uncertainty of the window expansion, as mentioned above. For the cases of 66 and 97 MeV/nucleon, the contributions of subtraction of the contaminants less than 0.4% were included as the systematic uncertainties. In Table II, the values of σ_R for ^{17}Ne on a proton target, which were obtained from previous experiments [36], are also listed at almost the same energies. The values of σ_R for ^{17}F on a proton target are almost the same as those of ^{17}Ne at the corresponding energies. In the next section, we discuss the experimental σ_R on a proton target in detail.

TABLE II. Experimental results for the total reaction cross sections (σ_R) for ^{17}F on a proton target along with those of ^{17}Ne measured previously using the SHT. For ^{17}F, the first and second parentheses in the third column indicate the statistical and systematic uncertainties, respectively.

Nucleus	Energy (MeV/nucleon)	σ_R (mb)	Data number in Table I
^{17}F	66	358.3(3.9)(3.8)	No.1, No.2
	97	319.4(1.9)(2.0)	No.3, No.4
	282	282.4(1.6)(1.5)	No.5, No.6
	461	296.5(2.1)(1.5)	No.7, No.8
^{17}Ne [36]	73	353.1(8.6)	
	100	322.6(5.9)	
	289	282.4(2.8)	
	432	300.2(2.2)	

IV. DISCUSSION

A. Glauber model calculations

Here, we evaluate σ_R of the ground state of ^{17}F on a proton target using a high-energy reaction theory, the Glauber model [43]. The wave function of ^{17}F is based on an ^{16}O$+p$ model. A harmonic-oscillator p-shell-closed configuration is assumed for the ^{16}O core, and it reproduces the experimental point-proton rms radius, 2.57 fm, extracted from Ref. [44]. The relative wave function of ^{16}O$+p$, ϕ_0 ($J^\pi = 5/2^+$), is generated by the phenomenological Woods-Saxon potential that reproduces both the one-proton separation energy $S_p =$ 600.27(25) keV [27] and the excitation energy of the first excited state of ^{17}F ($J^\pi = 1/2^+$). The resulting values of r_p, r_n, and r_m for the ground state of ^{17}F are 2.69, 2.58, and 2.64 fm, respectively. The thickness of the neutron skin is -0.11 fm. We also calculated these radii for the first excited state of ^{17}F. Those values are 2.96, 2.59, and 2.79 fm, respectively; they correspond to a larger extension of the proton radius and to a one-proton halo structure in the excited state.

Using the ^{17}F wave function thus obtained, we calculated σ_R on the basis of the Glauber approximation [43] as

$$\sigma_R = \int d\boldsymbol{b}(1 - |e^{i\chi(\boldsymbol{b})}|^2), \tag{2}$$

where b is the impact parameter. The optical-phase shift function [45] is given by

$$e^{i\chi(\boldsymbol{b})} = \int d\boldsymbol{r}\,|\phi_0(\boldsymbol{r})|^2 e^{i\chi_{CT}(\boldsymbol{b}-\frac{1}{17}\boldsymbol{s})+i\chi_{pT}(\boldsymbol{b}+\frac{16}{17}\boldsymbol{s})}, \tag{3}$$

where $\boldsymbol{r} = (\boldsymbol{s}, z)$ is the relative coordinate between the ^{16}O core and the proton with z being the beam direction. For a proton target ($T = p$), the optical-limit approximation (OLA) is employed to evaluate the optical phase-shift function of nucleon-nucleus scattering. The OLA works well for describing nucleon-nucleus scattering for stable nuclei, where the

multiple scattering effect can be ignored [46–49]. The explicit form of the core-p (Cp) optical-phase shift function is [43,45]

$$i\chi_{Cp}(\boldsymbol{b}) = -\int d\boldsymbol{r}'\left[\rho_p^C(\boldsymbol{r}')\Gamma_{pp}(\boldsymbol{b}-\boldsymbol{s}') + \rho_n^C(\boldsymbol{r}')\Gamma_{np}(\boldsymbol{b}-\boldsymbol{s}')\right], \tag{4}$$

where $\boldsymbol{s}'$ is the single-particle two-dimensional coordinate from the center of mass of the projectile nucleus perpendicular to the beam direction and ρ_p^C (ρ_n^C) is the proton (neutron) density of the ^{16}O core. The Γ_{NN} ($\Gamma_{pp} = \Gamma_{nn}$ and $\Gamma_{np} = \Gamma_{pn}$) is the profile function, which describes the nucleon–nucleon collision. The explicit form of the profile function is given in Ref. [50]. Note that $e^{i\chi_{pp}(\boldsymbol{b})}$ in Eq. (3) is nothing but $1 - \Gamma_{pp}(\boldsymbol{b})$.

For a carbon target, we employ the nucleon-target profile function in the Glauber model (NTG) [51,52] as

$$e^{i\chi_{CT}(\boldsymbol{b})} \approx \exp\left\{-\int d\boldsymbol{r}'\left[\rho_p^C(\boldsymbol{r}')\Gamma_{pT}(\boldsymbol{s}'+\boldsymbol{b}) + \rho_n^C(\boldsymbol{r}')\Gamma_{nT}(\boldsymbol{s}'+\boldsymbol{b})\right]\right\} \tag{5}$$

with

$$\Gamma_{NT}(\boldsymbol{b}) = 1 - \exp\left\{-\int d\boldsymbol{r}''\left[\rho_p^T(\boldsymbol{r}'')\Gamma_{Np}(\boldsymbol{b}-\boldsymbol{s}'') + \rho_n^T(\boldsymbol{r}'')\Gamma_{Nn}(\boldsymbol{b}-\boldsymbol{s}'')\right]\right\}, \tag{6}$$

where ρ_N^T is the density distribution of the target nucleus. Note that the symmetrized expression on the projectile and target nuclei is used. A harmonic-oscillator-type density distribution, which reproduces the experimental point-proton radius, 2.33 fm, extracted from Ref. [44], is used for a carbon target. The inputs to the NTG are the same as those to the OLA, but multiple scattering contributions are effectively considered. The validity of this approach has been well tested [47,48,52–56] and used as a standard tool to extract r_m of exotic nuclei [57–59]. The proton-target optical phase-shift function $e^{i\chi_{pT}}$ is evaluated by the OLA using Eq. (4) by replacing ρ^C with the target density distribution ρ^T.

An advantage of this formalism is that one can incorporate the core+p structure appropriately in the reaction process and that the inelastic scattering process can also be described in the same footing. Note that the interaction cross section σ_I is actually measured in this study. As ^{17}F has one bound excited state with $J^\pi = 1/2^+$, we need to evaluate the inelastic scattering cross section to the bound excited $J^\pi = 1/2^+$ state to compare the measured σ_I directly with the theoretical σ_R. The inelastic scattering cross section can be evaluated by replacing $|\phi_0(\boldsymbol{r})|^2$ in Eq. (3) with $\phi_{\rm ex}^*\phi_0$ and integrating $|e^{i\chi(\boldsymbol{b})}|^2$ over $\boldsymbol{b}$, where $\phi_{\rm ex}$ is the excited bound-state wave function of ^{16}O+p with $J^\pi = 1/2^+$. The resulting cross section values are found to be small at most 0.1 mb at the energy higher than 200 MeV/nucleon for a proton target. In general, the inelastic scattering cross section is larger at low energies. However, only 0.7 mb is obtained even at 40 MeV/nucleon. Therefore, the assumption $\sigma_I = \sigma_R$ holds safely in this case.

B. Target dependence of σ_R

Figure 4 compares the experimental and theoretical cross sections for ^{17}F on carbon and proton targets. Figure 4(a) shows good agreement between the theory and experiment for a carbon target. In contrast, for a proton target in Fig. 4(b), the calculated σ_R overestimates the experimental σ_R at low incident energies below 100 MeV/nucleon and slightly underestimates the experimental ones at higher incident energies $\gtrsim$200 MeV/nucleon. This energy dependence is similar to that observed for ^{17}Ne [36], which we discuss later. The nuclear size of the ^{16}O core in ^{17}F is not necessarily the same as that of the bare ^{16}O because of the interaction between the core nucleus and the valence nucleon. As the uncertainties in the carbon-target data for ^{17}F are large, ^{17}F may actually have a smaller radius. We therefore generated another version of the ^{17}F density by changing the radius of the ^{16}O core by -0.1 fm. The resulting values of r_p, r_n, and r_m for ^{17}F are 2.62, 2.48, and 2.56 fm, respectively, which is consistent with the result of earlier analysis ($r_m = 2.54 \pm 0.08$ fm [33]). Hereafter, we consider this to be the appropriate density distribution of ^{17}F. In Fig. 4(a), the calculated σ_R is found to be more consistent with the experimental data on a carbon target. However, for a proton target in Fig. 4(b), reproduction of the experimental σ_R at low and high incident energies seems to be difficult in this theoretical framework. The consideration of other complicated effects beyond adiabatic approximation, such as Pauli blocking, may be needed to provide a better explanation of the low-energy data.

To understand the properties of the nucleus-proton collision in more detail, we compared the cross sections of ^{17}F and ^{17}Ne. Figure 5 shows the experimental and theoretical cross sections of ^{17}F and ^{17}Ne. Here, the experimental and theoretical results for ^{17}Ne are taken from Ref. [36]. For a fair comparison, same approximations should be used for σ_R calculations for ^{17}F and ^{17}Ne; that is, the NTG for a carbon target and the OLA for a proton target, which are realized by using the phase-shift functions of Eqs. (4) and (5) for proton and carbon targets, respectively, with the density distribution of ^{17}F constructed from the ^{16}O+p wave function described in Ref. [52]. The difference from the present theoretical model based on Eq. (3) is not large for ^{17}F, at most about 1% for a carbon target and 3% for a proton target. Therefore, no qualitative difference is expected in the present analysis. For a carbon target in Fig. 5(a), the theoretical σ_R values consistently describe the cross-section data at low and high incident energies. σ_R of ^{17}Ne is larger than that of ^{17}F, reflecting the difference in their r_m: 2.68 fm [36] for ^{17}Ne and 2.56 fm for ^{17}F. In contrast, for a proton target in Fig. 5(b), the experimental results of ^{17}F and ^{17}Ne are similar at around the corresponding incident energies. The calculated σ_R explains the experimental trend: σ_R of ^{17}F is slightly larger than that of ^{17}Ne below $\approx$400 MeV/nucleon and similar at the higher incident energies. This target dependence is partly attributed to the isospin asymmetry of $\sigma_{NN}^{\rm tot}$, i.e., $\sigma_{pn}^{\rm tot}$ is around three times larger than $\sigma_{pp}^{\rm tot}$ below $\approx$100 MeV/nucleon. For a carbon target, the asymmetry dependence of $\sigma_{NN}^{\rm tot}$ is negligible because ρ_p and ρ_n of the target nucleus are virtually similar. On the other hand, a proton target is particularly sensitive to

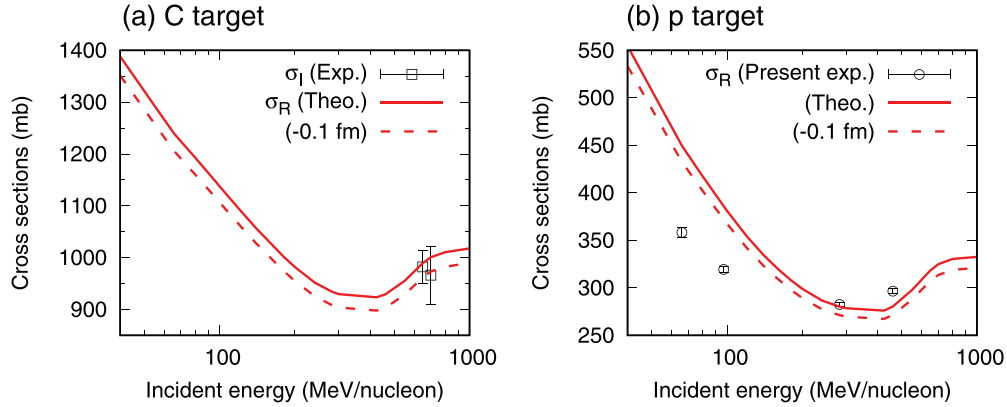

FIG. 4. Total reaction cross sections (σ_R) for ^{17}F on (a) carbon and (b) proton targets. The solid and dashed lines indicate the theoretical calculations of σ_R assuming the size of ^{16}O core extracted from the experimental value [44] and the size changed by -0.1 fm, respectively. The experimental data of the interaction cross section (σ_I) for ^{17}F on a carbon target are taken from Ref. [33].

neutrons in the projectile because of the asymmetry dependence of $\sigma_{NN}^{\rm tot}$, i.e., $\sigma_{pp}^{\rm tot} < \sigma_{pn}^{\rm tot}$ at incident energies below ≈500 MeV/nucleon. This sensitivity was theoretically quantified in Ref. [60]. Although r_m of ^{17}Ne is larger than that of ^{17}F, the difference for a proton target between σ_R of ^{17}Ne and ^{17}F becomes smaller than that for a carbon target because the neutron number of ^{17}Ne is smaller than ^{17}F. This finding is consistent with the discussions given in Refs. [37,38]: σ_R on a proton target decreases despite the increase of r_m toward the proton dripline for proton-rich carbon isotopes.

C. Reaction probability

The two-proton halo character of ^{17}Ne affects the behavior of σ_R. Figure 6 shows the reaction probability $P(b) = 1 - |e^{i\chi(\boldsymbol{b})}|^2$ as a function of the impact parameter b. For a carbon target, the reaction probabilities of ^{17}Ne exceed those of ^{17}F beyond ≈6 fm, showing a characteristic behavior due to the halo tail. As discussed in Ref. [38], since the complete absorption reaction in the sense of an optical model occurs within the radius where the two colliding nuclei interact, only the tail part of the density distribution can contribute to the difference between the cross sections of ^{17}F and ^{17}Ne. Comparing $P(b)$ at 200 and 800 MeV/nucleon, the incident-energy dependence is negligible.

On the other hand, for a proton target, the probabilities of ^{17}F are larger than those of ^{17}Ne in the internal region $2 \lesssim b \lesssim 4$ fm, while the opposite behavior occurs for $b \gtrsim 4$ fm. As discussed in Ref. [38], for light nuclei, there is a probability that the target proton can penetrate the projectile nucleus even at a small impact parameter; thus, the proton target has some sensitivity to the density profiles in the internal region. The contribution of the proton tail of ^{17}Ne becomes larger at 800 MeV/nucleon than that at 200 MeV/nucleon because $\sigma_{pp} > \sigma_{pn}$ holds at 800 MeV/nucleon, whereas $\sigma_{pp} < \sigma_{pn}$ at 200 MeV/nucleon.

D. Energy dependence of σ_R

Finally, we discuss the energy dependence of σ_R for ^{17}F and ^{17}Ne on a proton target. As shown in Fig. 5(b), for ^{17}F, the experimental σ_R at 282 and 461 MeV/nucleon (66 and

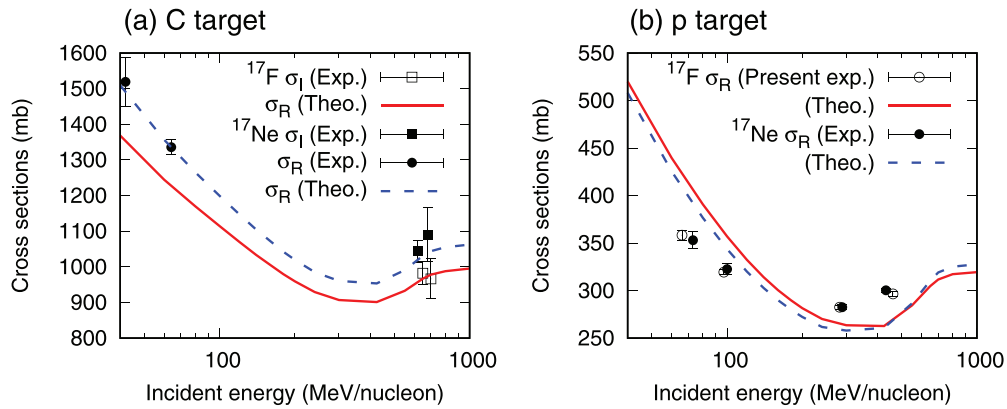

FIG. 5. Total reaction cross sections (σ_R) for ^{17}F and ^{17}Ne on (a) carbon and (b) proton targets. The experimental and theoretical σ_R of ^{17}Ne were taken from Refs. [6,36,61]. Similar to the ^{17}Ne case, to provide a fair comparison, theoretical σ_R for ^{17}F on carbon and proton targets were also calculated by using the NTG and the OLA, respectively, with the density distribution of ^{17}F. Note that the value of r_m of ^{17}F used for the calculation is 2.56 fm, which assumes the radius of the ^{16}O core to be changed by -0.1 fm from the experimental value [44].

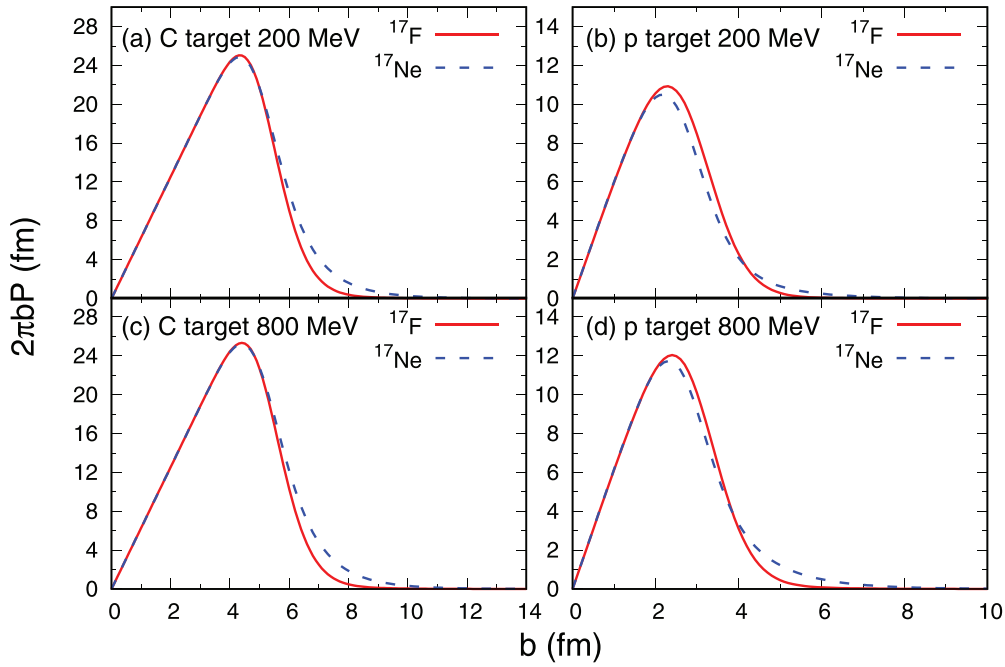

FIG. 6. Reaction probabilities of ^{17}F and ^{17}Ne on (a),(c) carbon and (b),(d) proton targets at incident energies of (a),(b) 200 and (c),(d) 800 MeV/nucleon as a function of the impact parameter b.

97 MeV/nucleon) are larger (smaller) than the theoretical one. This trend of ^{17}F is similar to that of ^{17}Ne, as pointed out in Ref. [36]: the experimental σ_R of ^{17}Ne on a proton target in intermediate and high (low) energies are larger (smaller) than calculated σ_R. In the previous study [36], this discrepancy of the energy dependence of σ_R on a proton target between experimental and theoretical σ_R was discussed carefully by considering contributions from the nuclear medium effect, the choice of the profile function, and the multiple scattering effect. Similar to ^{17}Ne, it appears to be difficult to explain the experimental σ_R of ^{17}F both on proton and carbon targets over a wide energy region using the present Glauber model. Further investigations are needed to understand the nucleus-proton collision in both experimental and theoretical sides.

V. SUMMARY

We measured the total reaction cross section (σ_R) for ^{17}F on a proton target to investigate the nucleus–proton collision for proton-rich nuclei. A thick and large solid hydrogen target, which is dedicated for σ_R measurements, was used as a proton target. We obtained the energy dependence of σ_R for ^{17}F on a proton target from several tens MeV/nucleon to several hundreds MeV/nucleon. We made cross-section calculations with the Glauber model and compared them with measured σ_R for the proton-dripline nuclei ^{17}F and ^{17}Ne.

For a carbon target, σ_R for ^{17}Ne is larger than that of ^{17}F owing to the large nuclear size of ^{17}Ne, which originates from the two-proton halo structure [6]. In contrast, for a proton target, measured σ_R of ^{17}F is almost the same as that of ^{17}Ne, even though the difference between the nuclear radii of the two nuclei is significant. This behavior can be understood by considering the fact that the isospin asymmetry of $\sigma_{NN}^{\rm tot}$ (i.e., $\sigma_{pp}^{\rm tot} < \sigma_{pn}^{\rm tot}$ below $\approx$ 500 MeV/nucleon) and the dilute proton density distribution of ^{17}Ne reduce the cross sections. This reduction is larger than the change of the cross section due to the increase of the nuclear radius. This finding is consistent with the theoretical investigation of proton-rich carbon isotopes [38].

The energy dependence of σ_R on a proton target is not yet fully understood. The experimental σ_R for ^{17}F on a proton target in low (high) energies are smaller (larger) than those obtained from the present theoretical calculations. This trend is similar to that of ^{17}Ne, which was carefully discussed in the previous study [36]. This discrepancy of σ_R on a proton target remains an open question. Further experimental and theoretical studies are needed to understand nucleus–proton collisions for precise determination of the proton- and neutron-size properties of atomic nuclei.

ACKNOWLEDGMENTS

We thank the AEC staff of HIMAC for steady operation of the accelerators and appreciate their technical support. This work was supported by the Research Project with Heavy Ions at QST-HIMAC (Project no. 16H365). We also thank M. Tanaka, D. Nishimura, and M. Fukuda for the fruitful discussions on the analysis and experimental results. This work was supported by JSPS KAKENHI (Grants No. JP16K17678, No. JP20K03997, and No. JP21H04461) and the University of Tsukuba Basic Research Support Program Type A (FY2019).

[1] M. Fukuda *et al.*, Nucl. Phys. A **656**, 209 (1999).
[2] T. Zheng *et al.*, Nucl. Phys. A **709**, 103 (2002).
[3] C. Wu *et al.*, Nucl. Phys. A **739**, 3 (2004).
[4] Y. Yamaguchi *et al.*, Phys. Rev. C **70**, 054320 (2004).
[5] M. Takechi *et al.*, Phys. Rev. C **79**, 061601(R) (2009).
[6] K. Tanaka *et al.*, Phys. Rev. C **82**, 044309 (2010).
[7] T. Yamaguchi *et al.*, Nucl. Phys. A **864**, 1 (2011).
[8] M. Takechi *et al.*, Phys. Rev. C **90**, 061305(R) (2014).
[9] D. Nishimura *et al.*, Nucl. Phys. A **834**, 470c (2010).
[10] T. Moriguchi *et al.*, Phys. Rev. C **88**, 024610 (2013).
[11] Particle Data Group, https://pdg.lbl.gov/ (2023).
[12] W. Horiuchi, S. Hatakeyama, S. Ebata, and Y. Suzuki, Phys. Rev. C **93**, 044611 (2016).
[13] W. Horiuchi, Y. Suzuki, T. Uesaka, and M. Miwa, Phys. Rev. C **102**, 054601 (2020).
[14] T. Yamaguchi *et al.*, Phys. Rev. C **82**, 014609 (2010).
[15] T. Yamaguchi, I. Hachiuma, A. Kitagawa, K. Namihira, S. Sato, T. Suzuki, I. Tanihata, and M. Fukuda, Phys. Rev. Lett. **107**, 032502 (2011).
[16] A. Estradé *et al.*, Phys. Rev. Lett. **113**, 132501 (2014).
[17] A. Ozawa *et al.*, Phys. Rev. C **89**, 044602 (2014).
[18] S. Terashima *et al.*, Prog. Theor. Exp. Phys. **2014**, 101D02 (2014).
[19] R. Kanungo *et al.*, Phys. Rev. Lett. **117**, 102501 (2016).
[20] D. T. Tran *et al.* (RCNP-E372 Collaboration), Phys. Rev. C **94**, 064604 (2016).
[21] K. Sawahata *et al.*, Nucl. Phys. A **961**, 142 (2017).
[22] S. Bagchi *et al.*, Phys. Lett. B **790**, 251 (2019).
[23] S. Kaur *et al.*, Phys. Rev. Lett. **129**, 142502 (2022).
[24] M. Tanaka *et al.*, Phys. Rev. C **106**, 014617 (2022).
[25] T. Moriguchi *et al.*, Nucl. Instrum. Methods Phys. Res. A **624**, 27 (2010).
[26] D. Tilley, H. Weller, and C. Cheves, Nucl. Phys. A **564**, 1 (1993).
[27] M. Wang, W. J. Huang, F. G. Kondev, G. Audi, and S. Naimi, Chinese Phys. C **45**, 030003 (2021).
[28] Z. Ren, A. Faessler, and A. Bobyk, Phys. Rev. C **57**, 2752 (1998).
[29] H. Y. Zhang *et al.*, Nucl. Phys. A **707**, 303 (2002).
[30] L. Yu-Jie, L. Xi-Han, Z. Hong-Yu, L. Zu-Hua, and D. Fu-Guo, Chin. Phys. Lett. **22**, 1086 (2005).
[31] Z. Dongmei *et al.*, J. Phys. G: Nucl. Part. Phys. **34**, 523 (2007).
[32] N. Patronis *et al.*, Phys. Rev. C **85**, 024609 (2012).
[33] A. Ozawa *et al.*, Phys. Lett. B **334**, 18 (1994).
[34] R. Morlock, R. Kunz, A. Mayer, M. Jaeger, A. Müller, J. W. Hammer, P. Mohr, H. Oberhummer, G. Staudt, and V. Kölle, Phys. Rev. Lett. **79**, 3837 (1997).
[35] G. Hagen, T. Papenbrock, and M. Hjorth-Jensen, Phys. Rev. Lett. **104**, 182501 (2010).
[36] T. Moriguchi *et al.*, Nucl. Phys. A **994**, 121663 (2020).
[37] K. Kaki, Prog. Theor. Exp. Phys. **2017**, 093D01 (2017).
[38] K. Makiguchi and W. Horiuchi, Prog. Theor. Exp. Phys. **2022**, 073D01 (2022).
[39] M. Kanazawa *et al.*, Nucl. Phys. A **746**, 393 (2004).
[40] H. Kumagai, A. Ozawa, N. Fukuda, K. Sümmerer, and I. Tanihata, Nucl. Instrum. Methods Phys. Res. A **470**, 562 (2001).
[41] K. Kimura *et al.*, Nucl. Instrum. Methods Phys. Res. A **538**, 608 (2005).
[42] V. G. Manzhelii and Y. A. Freiman, *Physics of Cryocrystals* (American Institute of Physics, New York, 1997).
[43] R. J. Glauber, *Lectures in Theoretical Physics* (Interscience, New York, 1959), Vol. 1, p. 315.
[44] I. Angeli and K. P. Marinova, At. Data Nucl. Data Tables **99**, 69 (2013).
[45] Y. Suzuki, R. G. Lovas, K. Yabana, and K. Varga, *Structure and Reactions of Light Exotic Nuclei* (Taylor & Francis, London, 2003).
[46] K. Varga, S. C. Pieper, Y. Suzuki, and R. B. Wiringa, Phys. Rev. C **66**, 034611 (2002).
[47] B. Abu-Ibrahim, S. Iwasaki, W. Horiuchi, A. Kohama, and Y. Suzuki, J. Phys. Soc. Jpn. **78**, 044201 (2009).
[48] T. Nagahisa and W. Horiuchi, Phys. Rev. C **97**, 054614 (2018).
[49] S. Hatakeyama and W. Horiuchi, Nucl. Phys. A **985**, 20 (2019).
[50] B. Abu-Ibrahim, W. Horiuchi, A. Kohama, and Y. Suzuki, Phys. Rev. C **77**, 034607 (2008).
[51] B. Abu-Ibrahim and Y. Suzuki, Phys. Rev. C **61**, 051601(R) (2000).
[52] W. Horiuchi, Y. Suzuki, B. Abu-Ibrahim, and A. Kohama, Phys. Rev. C **75**, 044607 (2007).
[53] W. Horiuchi and Y. Suzuki, Phys. Rev. C **74**, 034311 (2006).
[54] W. Horiuchi, Y. Suzuki, P. Capel, and D. Baye, Phys. Rev. C **81**, 024606 (2010).
[55] W. Horiuchi, T. Inakura, T. Nakatsukasa, and Y. Suzuki, Phys. Rev. C **86**, 024614 (2012).
[56] W. Horiuchi, T. Inakura, T. Nakatsukasa, and Y. Suzuki, JPS Conf. Proc. **6**, 030079 (2015).
[57] R. Kanungo *et al.*, Phys. Rev. C **83**, 021302(R) (2011).
[58] R. Kanungo *et al.*, Phys. Rev. C **84**, 061304(R) (2011).
[59] S. Bagchi *et al.*, Phys. Rev. Lett. **124**, 222504 (2020).
[60] W. Horiuchi, Y. Suzuki, and T. Inakura, Phys. Rev. C **89**, 011601(R) (2014).
[61] A. Ozawa, T. Suzuki, and I. Tanihata, Nucl. Phys. A **693**, 32 (2001).